Thermal Measurement Technique of Rib Elements on DSN Antenna Structure

S. Glazer
Applied Mechanics Technology Section

G. Gale
DSN Engineering Section

Thermal gradients on large DSN antennas may cause small structural deflections which affect the RF gain. These deflections may become very important at the high frequencies encountered in the Ka band. This report discusses an experimental test method employing an imaging infrared radiometer, which promises to yield accurate thermal data for these large antennas in a timely and convenient manner. The ultimate goal is to use the data in structural analysis codes to determine the effects on dish deflection and RF performance. Basic radiometric theory is presented, along with a description of the test apparatus and current experimental test procedures. A sample set of antenna rib temperatures using the developed methodology is also presented.

I. Introduction

Changes in length of rib elements on DSN antennas may cause the surface shapes to change enough to affect the RF gain. This is especially true if the antenna is to be used in the Ka band. A change in surface shape by as little as 1/50 of the wavelength (0.2 mm) will affect the gain. Complex shadow and illumination patterns resulting whenever the antenna does not track the sun may cause local rib temperature variations, which may in turn induce member strains. These complex thermal patterns are further affected by the transient tracking path, daily and seasonal weather conditions, and antenna geometry. This report describes an infrared radiometric technique for measuring antenna rib structure temperatures without attaching thermometers or thermocouples to the ribs. The data will subsequently be used as input to structural analysis codes to determine antenna surface deflections.

Several years ago an attempt was made to measure thermal gradients within the rib structure by attaching many thermocouples at the joint points and midway along the rib members. Data obtained from these measurements were inconsistent and data reduction was abandoned.

The present method employs a real-time infrared radiometer operated in the near infrared region to view the thermal emissions from the ribs. The IR signal is recorded on a standard video tape recorder, allowing a large quantity of data

to be obtained in a short period of time, and subsequent off-line data reduction. The advantages of this method are that thermal changes during the data taking period are held to a minimum, hardware which could interfere with normal use need not be attached to the antenna, and data analysis may be accomplished at a later, more convenient time.

II. Description of Infrared Radiometry

This section presents some of the background required for an understanding of the basic infrared radio metric method. This background includes a brief discussion of the fundamentals of radiation heat transfer, general principles of radiometer operation, and some of the factors which affect instrument accuracy.

A. Fundamentals of Radiation Heat Transfer

All objects whose temperatures are above absolute zero emit energy by the mechanism of radiation. This energy may be considered as being emitted in discrete packets sometimes called photons. Each photon also has an associated wavelength. A "black body" is defined as an object which emits the maximum possible theoretical energy over all wavelengths. The spectral radiant emittance is defined as the theoretical maximum energy flux which may be emitted at any wavelength λ by a black body at temperature T. The expression for the spectral radiant emittance is:

$$\text{Spectral Radiant Emittance } e = \frac{3.75 \times 10^{-12}}{\lambda^5 \left(e^{1.438/\lambda T} - 1\right)} \quad \frac{W}{\text{cm}^2\text{-}\mu\text{m}} \tag{1}$$

where

λ = wavelength in cm

T = temperature in K

Figure 1 graphically displays the spectral radiant emittance as a function of wavelength for black bodies of various temperatures. For many practical purposes, the sun may be considered a black body radiating at approximately 6000 K. As may be seen, the wavelength of maximum energy emission is approximately 0.5 μm, conveniently well within the narrow wavelength band to which our eyes are sensitive (the visible portion of the electromagnetic spectrum ranges from about 0.4 μm, to 0.7 μm). Cooler black objects emit less energy in the visible portion of the spectrum. In fact, as black body temperature decreases, the wavelength of peak energy emission increases. As seen in Fig. 1, black objects at room temperature emit nearly all their energy between about 4 and 30 μm, peaking at approximately 10 μm. Our eyes are therefore not sensitive to the energy emitted by room temperature objects; rather, they may be seen only by virtue of shorter wavelength energy (as for example, from the sun or artificial light sources) reflected from the surface. Infrared radiometers are generally sensitive to energy of wavelengths longer than 0.7 μm (infrared, or beyond the red, wavelengths).

As will be discussed shortly, the infrared radiometer used in the present study belongs to an important class of instruments which are sensitive not to the total energy emitted, but rather to the total number of photons striking the detector element. If we redefine the spectral radiant emittance as the maximum theoretical photon flux at any value of wavelength, then the following expression may be developed:

$$\text{Spectral radiant emittance } p = \frac{1.89 \times 10^{7}}{\lambda^4 \left(e^{1.438/\lambda T} - 1\right)} \quad \frac{\text{photons}}{\text{sec-cm}^2\text{-}\mu\text{m}} \tag{2}$$

where

λ = wavelength in cm

T = temperature in K

Figure 2 is a plot of this parameter as a function of wavelength for several black bodies of various temperatures.

In practice, black bodies do not exist. If emissivity is defined as the ratio of actual energy flux (or photon flux) emission per unit wavelength to the maximum theoretical (black body) rate, the emissivity of various surfaces would be found to depend on the wavelength, surface temperature, and direction of emission. For many real surfaces, the diffuse grey body approximation is made. A grey body is assumed to emit a constant fraction of the maximum theoretical energy at each wavelength. Further, the energy emitted by a diffuse grey body per unit projected surface area is assumed independent of direction. Emissivity defined in this way is often called the total hemispherical emissivity. Frequently, thermal analysis requires the dual grey body approximation, where two values of hemispherical (average) emissivity are used, one value for shorter wavelengths where the solar energy and photon emission peaks ($< \sim 4$ μm) and one value for longer wavelengths, where nearly all the energy and photon emission from room temperature objects occur ($> \sim 4$ μm). The former quantity is usually referred to as the solar absorptivity (α_s), and the latter simply as the emissivity (ϵ).

Energy and photons incident upon a surface may be absorbed, reflected, or transmitted through the surface. In general, each of these quantities is a function of wavelength, surface temperature, and direction. It may be shown that in the steady state, the directional, spectral emissivity of a

surface at temperature T equals the directional, spectral absorptivity of that surface. This is known as Kirchoff's Law. If the following definitions are made:

α = absorptivity = total fraction of incident energy absorbed

ρ = reflectivity = total fraction of incident energy reflected

τ = transmissivity = total fraction of incident energy transmitted through,

then it may be seen that

$$\alpha + \rho + \tau = 1 \tag{3}$$

If the surface is opaque to all radiation, then

$$\alpha + \rho = 1 \tag{4}$$

If Eq. (1), the spectral radiant emittance for a black body, is integrated over all wavelengths, then the total energy flux (called the black body emissive power, e_{bb}) is:

$$e_{bb} = \sigma T^4 \tag{5}$$

where σ is the Stefan-Boltzmann constant. For a real room temperature body assumed to be diffuse having a total hemispherical emissivity ϵ, the emissive power is

$$e = \epsilon \sigma T^4 \tag{6}$$

Thus the total energy leaving a surface per unit time and surface area is defined as the radiosity R, as

$$R = \epsilon \sigma T^4 + \frac{\text{(incident energy)}}{\text{unit-time-area}} \times \rho \tag{7}$$

Kirchoff's law in conjunction with Eq. (4) for an opaque surface indicates that Eq. (7) may be rewritten as

$$R = \epsilon \sigma T^4 + \left(\frac{\text{incident energy}}{\text{unit time-area}} \right) \times (1 - \epsilon) \tag{8}$$

A relation similar to Eq. (8) may be derived for the photon flux radiosity. Equation (8) states that the energy (and number of photons) leaving a surface is composed of two parts: that emitted and that reflected. The closer the surface emissivity to 1.0, the smaller the relative importance of the reflected 'component. Surfaces of many organic materials, including paints, have emissivities in the 0.8-0.95 range. A more complete discussion of radiation heat transfer may be found, for example, in Ref. 1.

B. Principles of Radiometer Operation

Radiometers may be divided into two general classes: those which sense the energy emitted (plus reflected), called thermal detectors, and those which detect the total number of photons emitted (and reflected), or photon detectors. Thermal detectors may employ the bolometric effect, as do thermistors and platinum RTD's, the thermovoltaic effect, (such as thermocouples and thermopiles), thermopneumatic or pyroelectric effects. Photon detectors may use the photovoltaic effect, as do solar cells, the photoconductive effect, or photoemissive effect.

The infrared radiometer used in the present analysis is a photon-sensitive device which utilizes the photoconductive effect. The electrical conductivity of this type of detector is a strong function of the photon flux. Since the detector does not respond to a change in its temperature, its speed of response is very fast, on the order of μsec. This type of detector is thus well suited to the rapid scene scanning necessitated by video compatible scan rates.

Single point sensing (nonscanning) and single horizontal line scanning infrared radiometers exist and are useful in certain applications. The most general and useful system is of the two-dimensional imaging type. Typically, photons from the scene are focused onto the small fixed detector element by means of rotating mirrors. The solid angle subtended by the detector is called the Instantaneous Field of View (IFOV), and is the smallest physical unit into which the scene may be resolved. It is also referred to as a resolution element. Photons from the overall scene being viewed, or Field of View (FOV), are focused sequentially onto the detector, resolution element by resolution element, until the entire scene has been scanned. After reference to some specified level, pointwise scene radiosities are displayed in a suitable manner, usually on a video monitor. In this format of data presentation, radiosity levels are usually indicated by local display brightness, with higher levels often displayed as brighter regions. Other modes of data presentation available with the specific instrument being used are discussed in Section III.

C. Factors Affecting Accuracy

Modern infrared radiometers infer object temperatures from radiosity levels observed. As previously discussed, radiosity, which is the total energy (or photon) flux leaving an object's surface, is composed of emitted plus reflected components. Only the emitted energy (or photon flux) component is meaningful in determining object temperature. It is

therefore necessary to separate the total radiosity into its constituents. In addition, infrared radiometer operation in an environment with absorbing and scattering media between the target and the instrument can further attenuate the radiosities measured. Finally, a large number of instrument-dependent properties, such as optical distortions, nonlinearity of detector signal amplification, electronic and radiometric noise, and detector and electronics transient response affect instrument accuracy. A brief discussion of the importance of some of these factors is included here. More complete treatments of this topic may be found in, for example, Refs. 2 and 3.

As previously discussed, all nonblack objects reflect some fraction of the energy incident upon them by other objects. The amount of energy incident upon the target (object whose temperature is to be measured) depends on (1) the temperature of the surrounding objects, (2) the view that the target surface has to each of the surrounding objects (or view factors), (3) diffusivity and specularity of all surfaces, (4) the emissivities of all the surrounding surfaces, and (5) the nature and quantity of all external energy (or photon) flux incident on all surfaces, i.e., the incident solar flux. In theory, all of the above factors must be known before target temperatures may be established with accuracy. Fortunately, physical test conditions of the present application, i.e., radiometric determination of thermal gradients on DSN antennas, permit use of many simplifying assumptions which eliminate the need for much of this detailed information. Following is a brief discussion of the simplifying assumptions being considered at this time in the final data reduction process.

The rib network comprising the antenna structure is highly complex and irregular. Any point on any rib member may have a physical view to several other rib elements, to the back of the dish surface, to the sky, and to the ground. All of these affect the incident energy and photon flux onto the target rib element. For the purpose of this analysis, the target rib will be assumed to view only the sky and the ground, not other portions of the antenna. This step is taken for several reasons. First, Eq. (8) indicates that the importance of energy or photons incident from other objects decreases as the target emissivity in the long infrared region ($> \sim 4\ \mu m$) approaches 1.0. The two types of white paint used on DSN antennas, Triangle #6 and Americoat #99, have emissivities in the 0.85-0.90 range; hence energy (or photons) from all other sources of approximately the same temperature contribute only 10-15% to the overall radiosity. Second, it is assumed that the view factor from the outward facing target rib elements to all other surrounding ribs is small in comparison with the total hemispherical view. It is therefore reasonable to assume that each target rib section views only the sky and the ground, each approximately equally. For simplicity, the ground and the sky may each be assumed "black," ($\epsilon \approx 1.0$) and the ground temperature set equal to the ambient air temperature. Correlations exist (Ref. 4) for clear sky effective temperature. The black body approximations for the sky and ground imply totally diffuse surfaces. Similarly, paints of the type used on the antennas typically are highly diffuse, and exhibit very small specular components. This assumption will be tested in the laboratory for the particular paints used. The use of these simplifications permits rib temperature determination without the necessity of complex thermal modeling.

The importance of reflected solar energy in the total radiosity measured will be ignored. Outside the earth's atmosphere, at a distance of 1 astronomical unit, the actual measured radiant emittance of solar radiation matches closely that of a black body at approximately 6000 K. However, the total energy / flux through air mass 1 (the solar intensity measured with the sun directly overhead) is approximately 1000 W/m^2. Beyond 7 μm, only about 0.2% of this energy, or 2.0 W/m^2 is detected. By contrast, a black object at 30°C emits approximately 157 W/m^2 between 7 and 12 μm. The diffusely reflected solar component from a target with an emissivity of 0.9 is thus less than 1.0% of the emitted energy in this wavelength band. For this reason, a spectral filter which prohibits energy and photons below 7 μm from passing will be used in conjunction with the infrared radiometer in future tests.

Transmission of energy through the earth's atmosphere is another factor affecting accuracy of radiometric measurements. In general, the mechanisms of absorption and scattering attenuate energy within the earth's atmosphere. The phenomenon of scattering causes collimated energy to be scattered diffusely. Effects of molecular scattering are negligible in the atmosphere for energy above about 2 μm, whereas scattering from clouds, aerosols, and hazes is not and must be considered when they intervene between the radiometer and the target.

Absorption is highly significant in attenuating energy or photon fluxes in the earth's atmosphere. In the phenomenon of molecular and gaseous absorption, energy is absorbed and reemitted at the molecule or gas temperature. In the lower atmosphere, water vapor, carbon dioxide, ozone, and methane are the primary constituents causing significant energy attenuation. The extent of spectral attenuation is highly dependent on such factors as the local concentrations of these components, humidity, pressure, target to radiometer distance, and altitude. While spectral transmission through the earth's atmosphere is highly nonuniform and variable, it is generally restricted to the 3.5-5.0 μm and the 8.0-14 μm bands within the 2-20 μm thermal energy wavelength region. Typical atmospheric spectral transmission curves as a function of many of the parameters mentioned are presented in Ref. 2.

Additional factors affecting the accuracy of radiometric temperature determination involve instrument specific operating characteristics. These factors include the specific detectivity of the detector, which is basically the detector output signal-to-noise ratio at 1 watt of monochromatic input power; the responsivity, which is the detector gain per watt of input energy; amplifier linearity, electronic noise, optical aberrations, internal reference level stability with time, and the relationship between target size, scene scan rate, and overall system response. Thorough explanation of these and other factors is beyond the scope of the present report, and so will not be treated here. References 2 and 3, for example, provide adequate coverage of these topics. Only the first and last of the above factors will be very briefly discussed here, due to their particular importance in the present application.

The specific detectivity D^* depends principally on the spectral sensitivity of the detector material, and is thus basically a material property. The specific detectivity of a system may be enhanced by detector operation at cryogenic temperatures. Many modern radiometers thus employ liquid nitrogen cooled detectors. The specific detectivity is an important consideration when choosing the optimal detector element for a particular application. Generally, the highest values of D^* are desirable at the wavelengths where most of the target energy (or photons) is emitted. Figures 1 and 2 indicate that objects around room temperature (such as in the present application) emit the most energy at the longer wavelengths, so that the detector D^* should be optimized in this region for the present application.

Target size is also a very important consideration in infrared radiometry. As discussed, the instantaneous field of view (IFOV), or resolution element, is the smallest size target which may be resolved. However, due to overall instrument response time, a step change in target temperature takes a finite amount of time to be accurately indicated on the display. Since the IFOV is constantly moving in a scanning system, this translates into a finite distance from the start of a uniform temperature region. At video scan rates, a general rule of thumb is that uniform temperature targets should occupy at least 4-5 IFOV's for accurate temperature indication.

D. Minimum Resolvable Temperature Difference– An Accuracy Criterion

The minimum resolvable temperature difference (MRTD) is a commonly used accuracy parameter for infrared radiometers. This criterion uses four bar targets of fixed aspect ratio, but variable widths. In the MRTD test, the black target foreground and background are maintained at fixed and well-known temperature differences. The MRTD at any given target size (expressed in terms of bar cycles/milliradian of scene) is the minimum ΔT between target foreground and background at which observers can distinguish the pattern through the electronic and radiometric noise. The MRTD is thus a curve which asymptotically approaches a single ΔT value. It is a useful tool in comparison of radiometric systems.

III. Description of the Infrared Camera Used

The infrared camera used is an Inframetrics Model 525 two-dimensional scanning radiometer. It uses a liquid-nitrogen-cooled HgCdTe detector element which is designed to be sensitive primarily to radiation in the 8-12 μm wavelength band. The system can measure temperatures over the range of -20 to +1300°C, with a minimum resolvable temperature difference (MRTD) of 0.1°C for a black 30°C target which is at least 5 IFOV's in size. Thermal images are presented in real-time on a television monitor, with regions of higher radiosity nominally appearing brighter. System output is compatible with RS-330 video, enabling real-time recording of thermal imagery on a conventional video tape recorder. Subsequent quantification of the thermal data may be performed off line by replaying the video tape through a colorizing system which artificially assigns false colors to a maximum of six radiosity intensity bands. The same colorizing system may alternately be used in a black and white mode to artificially highlight all regions of the scene displaying the same selectable value of radiosity. It is this mode which permits most convenient scene temperature comparisons with a known reference. Further discussions of data analysis procedures are contained in Section IV.

The basic infrared radiometer without magnification optics has an instantaneous field of view (IFOV) of 2.0 mr, and an overall field of view (FOV) of 14 × 18°. Guidelines discussed in Section II indicate that the smallest target for which temperatures may be accurately determined occupy 5 IFOV's. Without optical magnification, this corresponds to a minimum target of 18.0 inches at a nominal radiometer-to-antenna distance of 150 feet. A 10X magnifying telescope attachment is therefore used in the present application. This accessory narrows the overall FOV to 1.4 × 1.8°, while reducing the IFOV to 0.2 mr. This causes a subsequent reduction in minimum target size to 1.8 inches at 150 feet, enabling accurate thermal resolution of the 2- to 3-inch-wide structural members. The 10X telescope has an 8-inch aperture, and uses both refractive and reflective optics. Descriptions of additional related equipment used in the thermal tests are provided in Section IV.

IV. Thermal Test Methodology

A. Initial Test Method

Throughout 1980 and 1981, a low level effort was conducted at the Goldstone DSCC to determine the feasibility

of infrared radiometry to yield meaningful antenna temperatures for subsequent use in structural analysis codes. Ground-based observations were made initially with the standard optics, and later, with a 3-power magnifier lens. These attempts proved fruitless, because the sizes of typical structural members on the Venus antenna (DSS 13) are too small for accurate thermal resolution from a distance of 150 feet, necessary for adequate ground-based spatial coverage. As discussed in Section II, a minimum of 5 IFOV's, or resolution elements, are required for accurate instrument response to a uniform temperature target. Further, the complex rib structure on the antenna made positive member identification with only the infrared image very difficult. Figure 3 is a wide angle picture, taken with a standard video camera, of the 32-m DSS 13. It illustrates the complexity of the rib structure. The subreflector and quadrupod legs may be seen through the perforated dish surface. These problems are magnified with the 64-m Mars antenna (DSS 14).

The next approach involved infrared inspection of structural members while based in a movable aerial work platform (a large cherry picker). Using this technique, the infrared instrument, operator, and platform operator conducted all operations from the cherry picker bucket, which was constantly maneuvered to within approximately 6 feet of the antenna structural members. This method yielded positive element identification and reasonable size views of much of the antenna. Figure 4 is an infrared image of a structural member taken from the cherry picker. This figure illustrates the iso-radiosity enhancement mode discussed in Section III.

The aerial survey technique included several serious drawbacks, however. Great care was required in platform maneuvering around the complex antenna structure, particularly during periods of antenna tracking. The requisite care in platform placement limited the speed of the overall data collection procedure to approximately one relatively complete thermal map every 3-4 hours. Contributing to the length was the requirement of moving the truck-based cherry picker to several positions around the antenna to obtain adequate coverage. Possible errors were introduced into the data gathered by this method by several factors. First, ambient conditions (i.e., air temperature, wind velocity, direction) could change appreciably over the several-hour test duration. Thus, initial data points could be taken under different conditions than those recorded near the test conclusion. Secondly, radiometer instrument internal reference level temperature may not have remained constant throughout the test. Typically, an external base level was established approximately once per hour by viewing a controlled black body reference source placed on the antenna. This may be inadequate and of questionable validity given the level of accuracy required.

B. Present Data Collection Method

The current test procedure again utilizes the infrared radiometer in a ground-based mode, but with a 10X magnifier lens. An adequate view of most of the antenna structure may be obtained from one, and at most two, fixed positions approximately 150 feet behind the antenna. The 10X telescope attachment, which is an off-the-shelf radiometer accessory, reduces the resolution element size to approximately 0.2 mr, so that a 2-inch-wide structural member occupies approximately 5.5 resolution elements, which will yield acceptable accuracy. Figure 5 is an infrared image of rib elements taken with the 10X telescope attachment from the ground. It is approximately the area indicated in the rectangle on Fig. 3. Additional magnification is possible by using the radiometer 2:1 electronic zoom. One drawback to the present system is that the extremely narrow total field of view of approximately $1.4 \times 1.8^{\circ}$ makes structural rib element identification extremely difficult with the infrared radiometer alone. For this reason, the present test procedure utilizes a standard video camera with a high magnification zoom lens hard-mounted to the same remotely controlled pan/tilt head as the infrared radiometer so that both systems may view approximately the same scene. Positive rib element identification is then established with the video image. Figure 6 is a photograph of this test assembly. The larger, black telescope attachment (seen on the left in Fig. 6) is the 10X infrared lens. Using this procedure, a relatively complete data set may be accumulated within approximately 15 minutes. It is felt that changes in ambient conditions and radiometer reference levels are acceptably small during this period.

Radiometer calibration is an important consideration in the present application. It is necessary to establish a known reference level against which rib radiosities may be measured. It is also necessary to accurately determine radiosity attenuation due to such factors as telescope optical transmissivity and spectral atmospheric absorption under the local, instantaneous conditions. Initial tests of the present method, described in section V, utilized a long, thick-wall aluminum tube, closed at one end, with a 2-1/2-inch-diameter aperture at the other end. The interior was painted with a flat black paint, and the exterior was heavily insulated. It was estimated that cavity emissivity was approximately 0.98, based on Ref. 3. Two thermocouples embedded in the closed end cap indicated the temperature. This "homemade," uncontrolled reference source was placed at the base of the antenna structure and viewed through the same optics from the same distance as the antenna structural members. The test procedure called for establishment of a reference level before the actual data collection. The radiometer sensitivity was adjusted so that temperature differences of approximately $16^{\circ}C$ on "black" objects at around room temperature without the telescope attachment would

cause the display of radiosity on the video monitor to vary from saturated black to saturated white, with 64 discrete grey levels in between. After the reference device reached a stable temperature (near ambient), a single reference level was established and recorded on videotape. The instrument was then used to measure and record on videotape radiosities of the antenna structural members. The base reference level was again checked after the data collection.

Calibration procedures in future tests will probably utilize a controlled black temperature reference source. Accuracy will be improved if a complete calibration curve, defining observed radiosity versus source temperature, is obtained under identical operating conditions. Simplifying assumptions discussed in section II will then be used to estimate the true emitted energy, and hence, actual rib temperatures.

V. Preliminary Results

An initial feasibility test was performed at the DSS 13 site on 7/30/81 utilizing the ground-based infrared inspection procedure outlined in section IV. The antenna was forced to track the anticipated sun position with a four-hour lead. The purpose was to attempt to keep approximately the same solar insolation and shadow pattern on the antenna and rib structure, while at the same time inducing a severe thermal gradient condition. As a result of the tracking offset, approximately 1/3 of the dish surface was directly illuminated, and the rest shadowed. A significant portion of the rib structure was also in the sun.

Figures 7 and 8 represent an isothermal map of DSS 13 rib structure under the test conditions indicated. Figure 7 indicates the temperatures on the rib elements directly beneath the dish surface; Fig. 8 indicates lower rib elements. Only about 1/2 to 2/3 of the antenna rib structure could be measured from the single IR camera ground position. Thermal data displayed are preliminary, and have not yet been fully reduced according to the assumptions and procedures outlined in Section II. Future tests will utilize more exact data reduction techniques, and may be taken from multiple ground positions to provide more complete spatial coverage (if required).

The entire surface of the antenna at DSS 13 is painted with a thermally diffuse white paint made by dissolving titanium oxide, zinc oxide, and diatomaceous silica in a modified polyester. The paint is white in the visible, so that it reflects most solar energy, but has a high emissivity in the longer infrared wavelengths. The rib structure below the antenna surface is also covered with this paint. However, there is a red painted band around the extreme outer rim of the antenna, and a much higher temperature at this edge was observed due to the increased solar absorptance of the red color. An unpainted steel platform was added below the rib structure, and a 5-10°C difference between the painted and unpainted surface was observed.

Figures 7 and 8 indicate maximum rib thermal gradients on the order of 6°C under the instantaneous ambient conditions. The data will be used in a structural computer code in an attempt to calculate thermally induced antenna surface deflections and resulting RF gain losses. Additional directions of the thermal test program are discussed in section VI.

VI. Conclusions and Future Work

Experience gathered to date with the infrared camera indicates that the radiometric technique may be used to provide accurate thermal gradient data about the large and complex antenna structures. Additional refinements to the overall test procedure are expected to further reduce the effort and cost of future analyses.

Current plans call for additional thermal analyses of the 32-m-diameter Venus antenna (DSS 13) while employing several different antenna solar tracking modes in the attempt to determine worst possible case thermal gradients. The relative speed of the method should enable thermal transient investigation over the course of a day. It is also planned to study the effects on thermal gradients under several environmental conditions throughout the year. Where possible, other antennas of varying sizes within the DSCC will be studied experimentally, and attempts will be made to correlate antenna size/complexity with observed thermal gradients. The study may also be extended to cover other portions of the antennas, such as the subreflector, quadrupod legs, etc. Structural/thermal analysis interface requirements will be defined to permit convenient use of thermal gradient data in a timely manner.

References

1. Siegel, R., and Howell, J., *Thermal Radiation Heat Transfer*, McGraw-Hill Book Company, 1972.
2. Lloyd, J. M., *Thermal Imaging Systems*, Plenum Press, 1975.
3. Wolfe, W. L., *The Infrared Handbook*, prepared for the Infrared Information and Analysis Center (IRIA), Environmental Research Institute of Michigan.
4. Ware, J. C., "Clear Sky Temperature," presented at the ISES Meeting, Fort Collins, Colorado, August 1974.

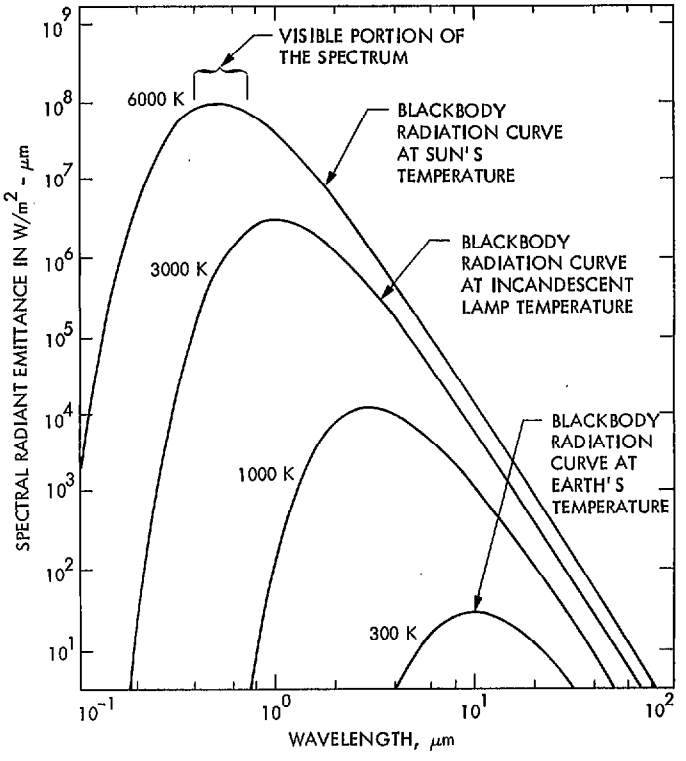

Fig. 1. Spectral distribution of energy radiated from a black body at various temperatures

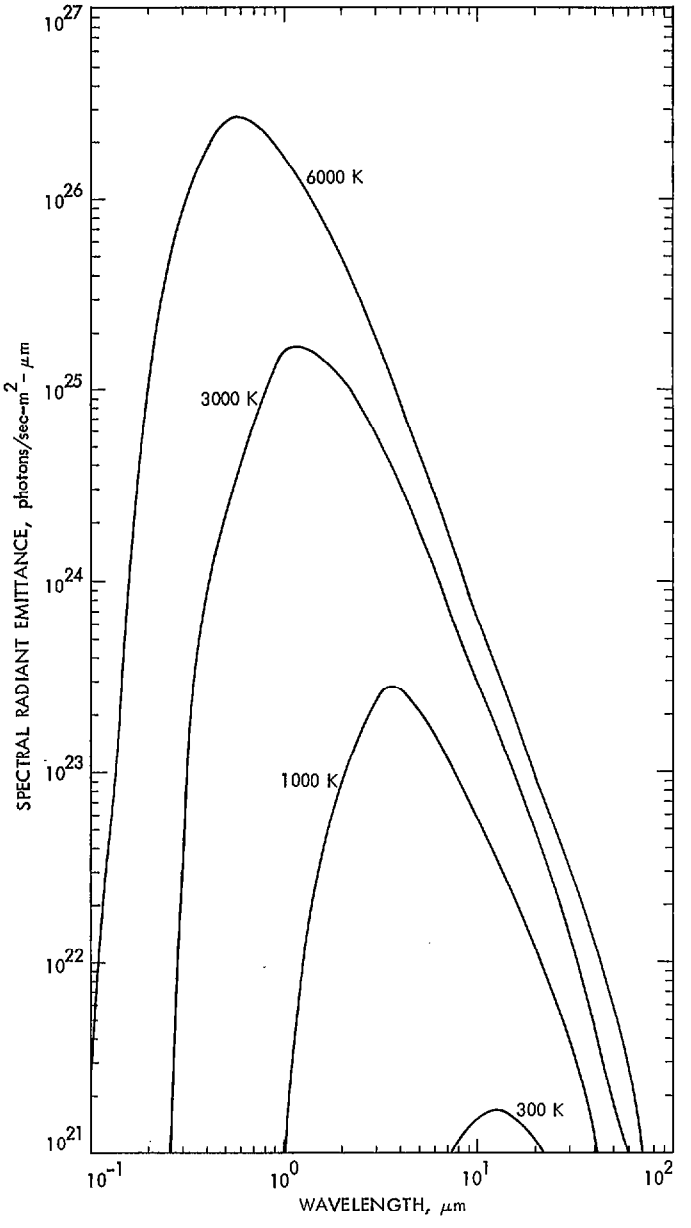

Fig. 2. Spectral distribution of photons radiated from a black body at various temperatures

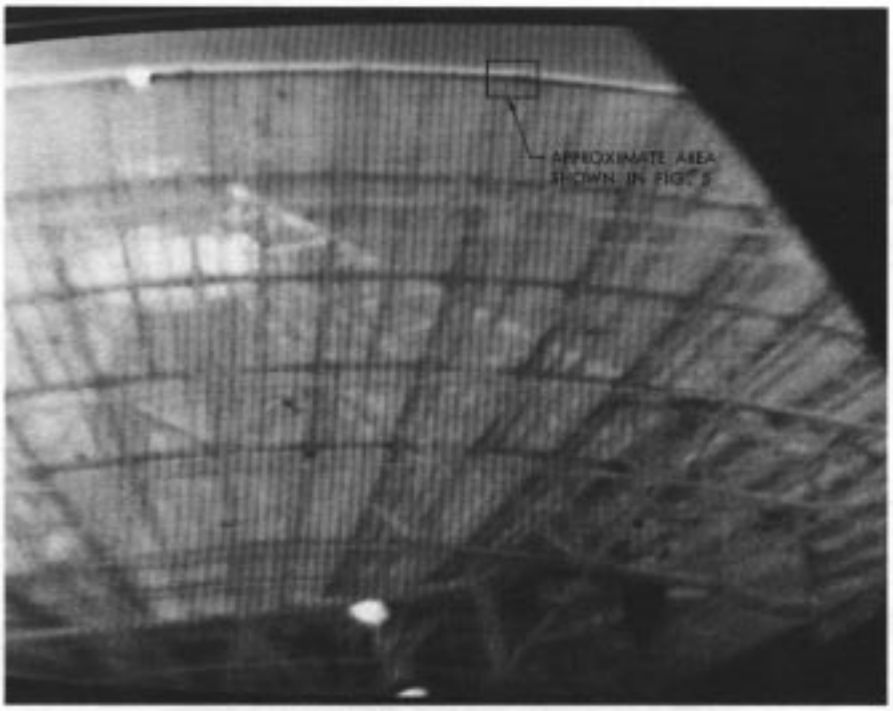

Fig. 3. Video picture of DSS 13

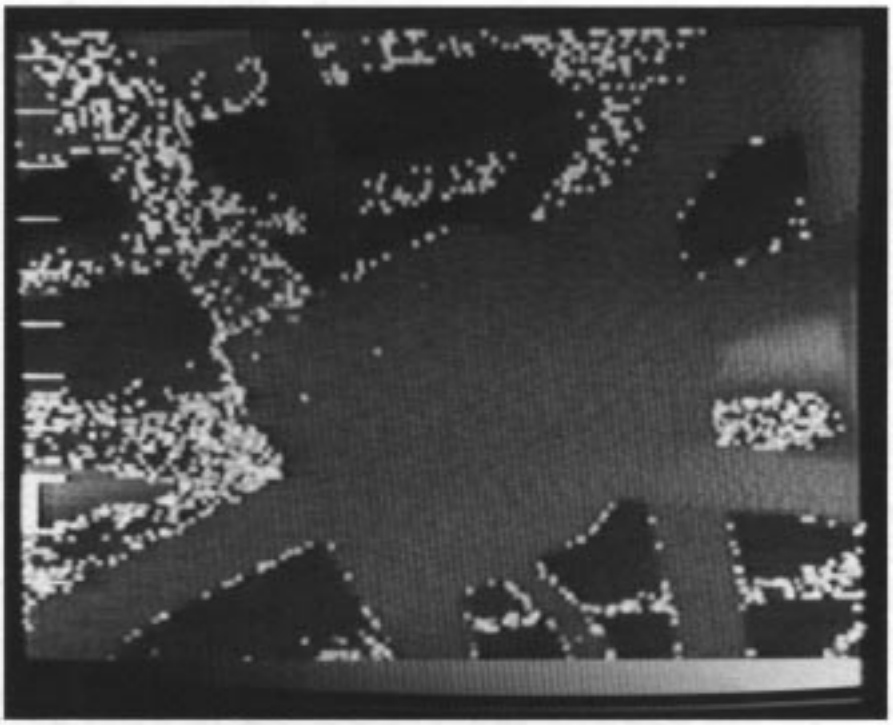

Fig. 4. Closeup infrared image of rib joint from cherry picker bucket, using iso-radiosity enhancement mode

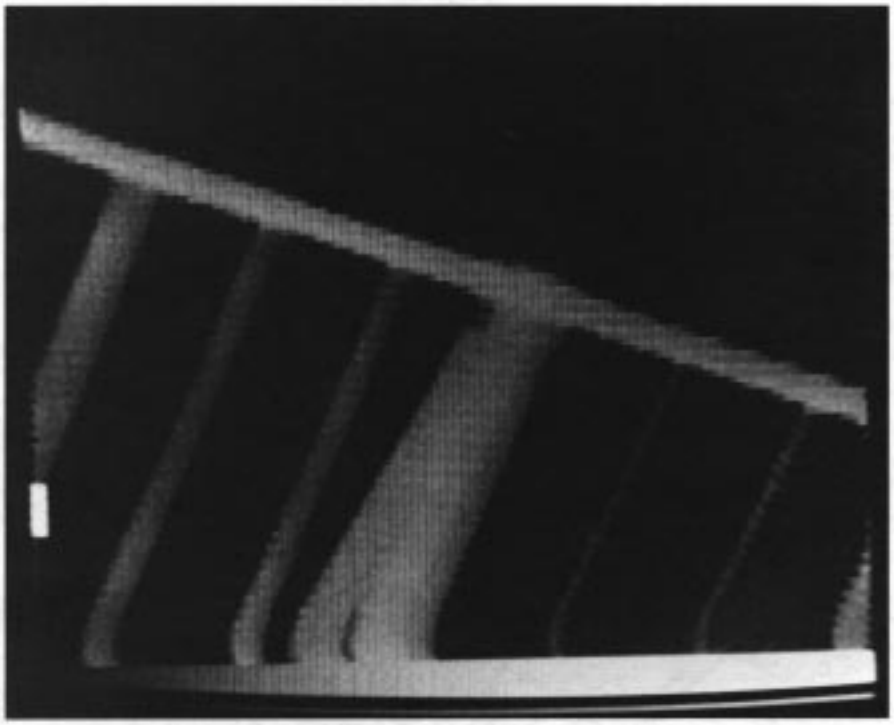

Fig 5. Infrared image of rib joint using ground-based 10× telescope from approximately 150-foot range

Fig. 6. Test assembly

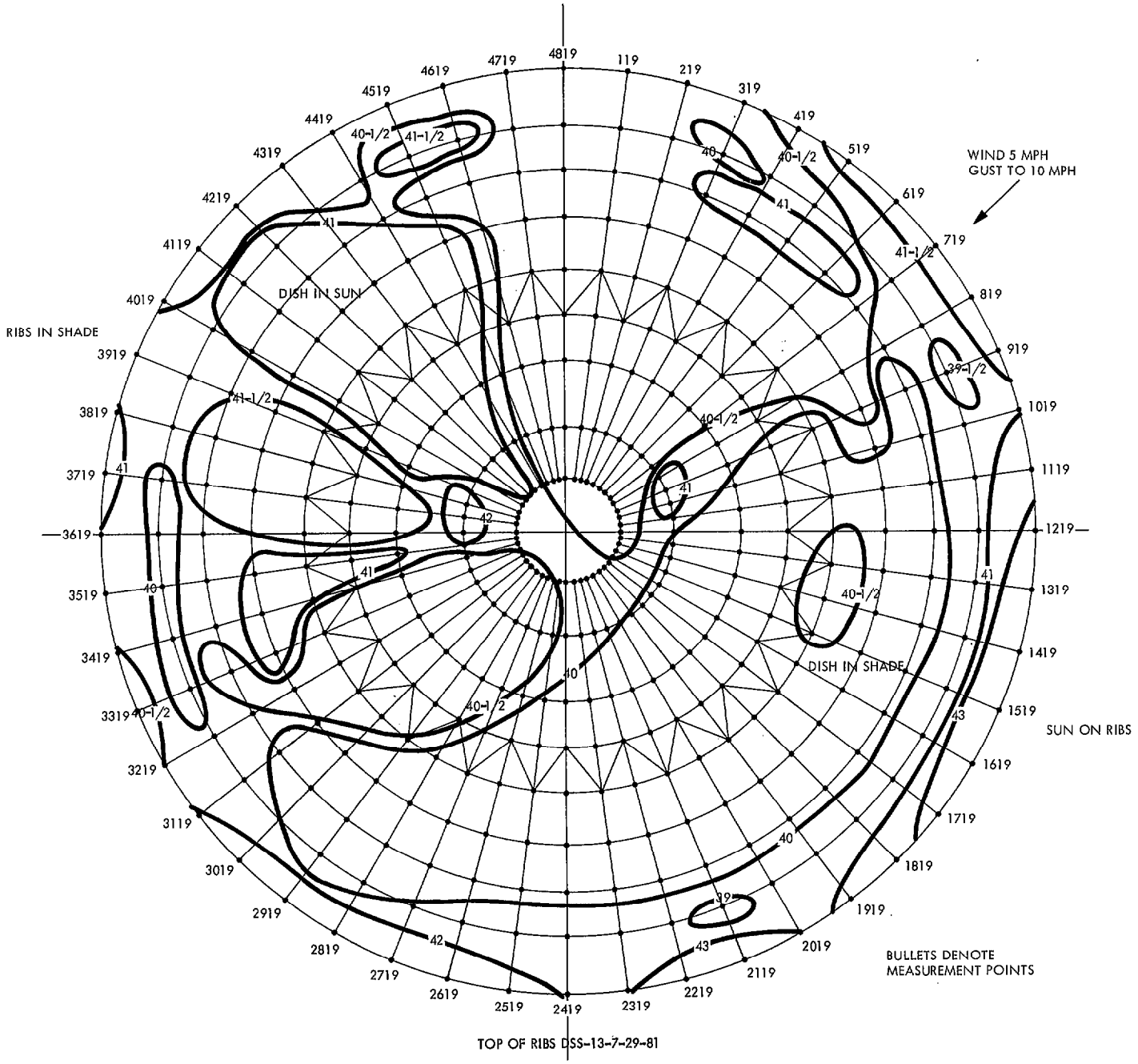

Fig. 7. Isothermal rib temperature map of DSS 13, for rib joints immediately beneath dish surface

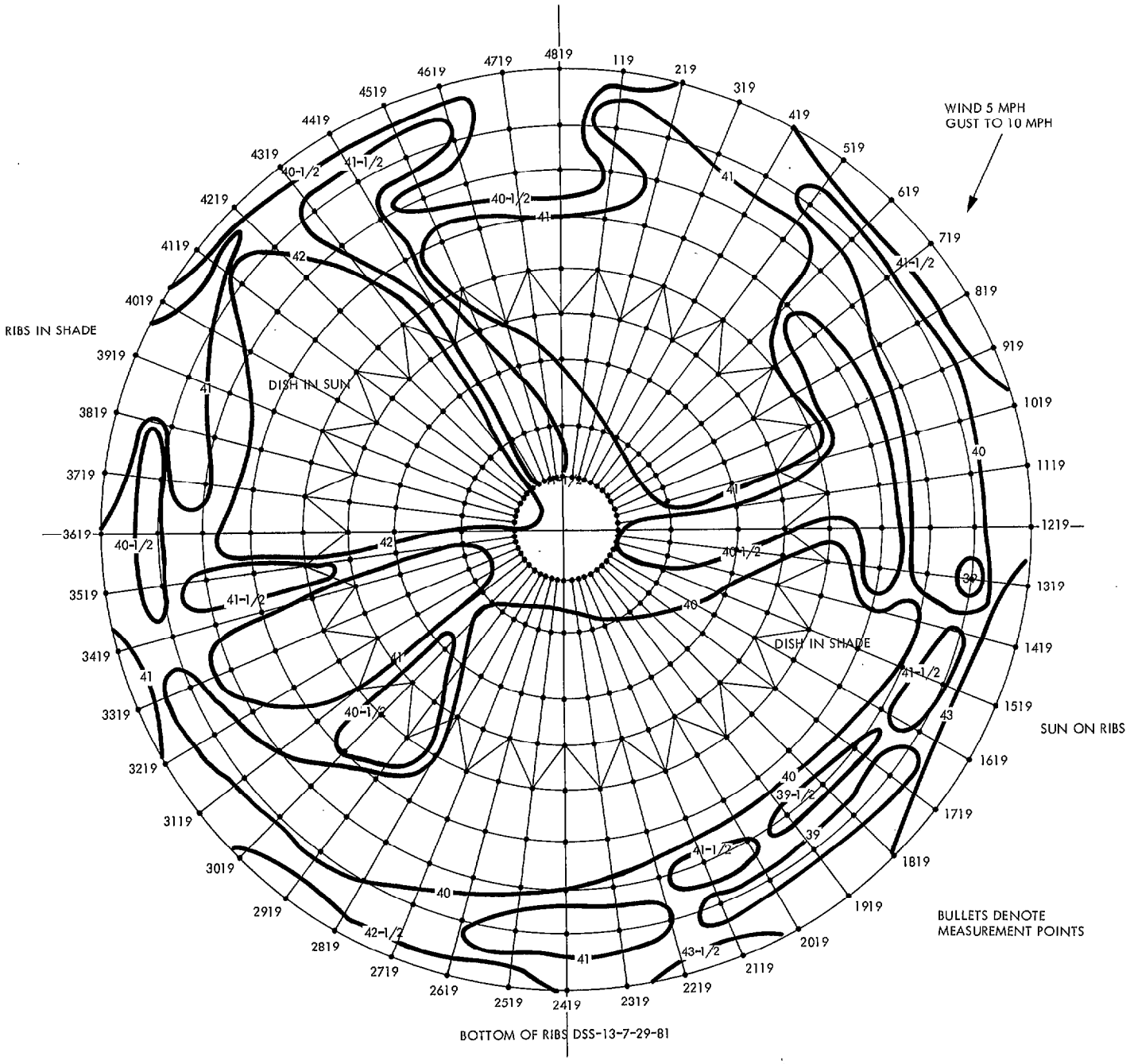

Fig. 8. Isothermal rib temperature map of DSS 13, for lower rib joints